J Mater Sci (2008) 43:2844–2848
DOI 10.1007/s10853-007-2384-1

Cathodoluminescence study of Te-doped ZnO microstructures grown by a vapour–solid process

A. Iribarren · P. Fernández · J. Piqueras

Received: 2 October 2007 / Accepted: 4 December 2007 / Published online: 11 January 2008

Abstract Sintering of a mixture of TeO_2 and ZnO powders under an Ar flux leads to the formation of elongated Te-doped ZnO nano- and microstructures on the sample surface. The growth of the structures occurs via a vapour–solid process. Cathodoluminescence (CL) and energy dispersive spectroscopy (EDS) measurements show an inhomogeneous incorporation of Te along the growth axis of the structures. An enhancement of the band edge emission upon Te doping is attributed to the passivation of oxygen vacancies by Te atoms, which reduces the deep energy level-related recombination path.

Introduction

Low-dimensional semiconductor structures, in particular of ZnO, are the subject of increasing interest due to their potential applications in several fields from optoelectronics to gas sensing or catalysis. Among the properties of this material, a wide direct band gap (3.37 eV) and a large exciton binding energy (60 meV) are playing a main role in a number of applications. However, the difficulty to prepare ZnO with p-type conductivity is hampering its extensive use in many electronic applications [1–3]. The role of defects in compensation mechanisms in bulk materials is in general well known, but in the doping of nanomaterials self-purification processes have been proposed to be determinant [4–6]. Recently, Erwin et al. [7] suggested instead that the adsorption of impurities on the nanocrystal surface during growth determines the efficiency of the doping process. Isovalent impurities in II–VI compounds produce several effects on their physicochemical characteristics [8]. In the case of Te-doped ZnO, passivation of O vacancies by Te atoms should be expected, since Te atoms could occupy both Zn and O sites.

In the present work, Te-doped ZnO elongated nano- and microstructures have been grown by thermal treatment of a compacted mixture of ZnO and TeO_2 powders under argon flow. This vapour–solid (VS) method has been reported to lead to the growth of elongated nanostructures of oxides such as ZnO [9], SnO_2 [10], Ga_2O_3 [11], GeO_2 [12] or In_2O_3 [13] on the surface of the sample so that neither a catalyst nor a foreign substrate is used. The obtained Te-doped ZnO structures have been characterized by X-ray diffraction (XRD), scanning electron microscopy (SEM), X-ray energy dispersive spectroscopy (EDS) in SEM and cathodoluminescence (CL) in SEM.

Experimental

The raw materials were ZnO (99.9%) and TeO_2 (99.9995%) commercial powders. Samples containing 1, 5 and 10 wt.% of TeO_2 were prepared by milling in a Retsch S100 centrifugal ball mill with 20 mm agate balls for 10 h. The milled powders were compacted under a 2 tons compressive load to form disc-shaped samples of about 7 mm diameter and 2 mm in thickness. The samples were then placed on an alumina boat near the gas inlet in a furnace,

A. Iribarren
Instituto de Ciencia y Tecnología de Materiales, Universidad de La Habana, Zapata y G, Vedado, Ciudad de La Habana 10440, Cuba

A. Iribarren · P. Fernández (✉) · J. Piqueras
Departamento de Física de Materiales, Facultad de Ciencias Físicas, Universidad Complutense de Madrid, 28040 Madrid, Spain
e-mail: arana@fis.ucm.es

and sintered at 1,270 °C under 2 L/mi argon flow for 15 h. Morphology and CL studies have been performed in a Leica 440 SEM. CL images were recorded by using a Hamamatsu R928 photomultiplier and CL spectra were obtained with a Hamamatsu PMA-11 CCD camera. XRD characterization of the samples was carried out in a Philips diffractometer working at 45 kV and 40 mA, using Cu $K\alpha$ radiation. X-ray microanalysis was performed using a JEOL JXA-8900 Superprobe by EDS.

Results and discussion

Different elongated microstructures have been observed on the sample surface after the thermal treatment. Their morphology has not been found to depend on the nominal Te content in the starting mixture. Some needle-like and pencil-like structures are similar to those grown by the same method in undoped ZnO [9, 14] while others, as those shown in Fig. 1, are characteristic of the doped samples. The arrows shown in Fig. 1, have a large range of sizes, corresponding to different stages of growth, and show an increasing cross-sectional dimension from the bottom to the top. The longer structures reach lengths of hundreds of microns.

The CL spectrum of undoped ZnO is very well known and consist of two main bands centred at about 3.3 and 2.5 eV related to band edge and defect levels, respectively. Deconvolution into Lorentzian curves shows the complex character of both bands. The different components of the low-energy band can be ascribed to several defects such as zinc vacancies [15], O vacancy-related centres [16, 17], or insterstitial Zn [18–20]. The ZnO band edge emission is centred at $h\nu_{max} \approx 3.26$ eV according to the values previously reported [19, 21, 22] and the typical width (FWHM) is about 0.10 eV. However, an additional component observed at 3.10 eV could be related to the contribution of defects such as dislocations [20, 20], interstitial Zn [19], or grain boundaries, which introduce a level at 0.33 eV below the conduction band [23].

Upon Te doping some changes in the CL emission are observed, however since the Te incorporation is not homogeneous, there is no apparent correlation between these changes and the nominal doping concentration. Nevertheless, the comparison of CL and EDS results indicates that some changes in CL spectra may be related to changes in Te incorporation.

CL spectra of the doped samples over a relatively wide surface region (Fig. 2), where no structures were grown, show a main intense peak in the violet region with the energy maximum shifted to energies lower than that of pure ZnO which can be related to Te doping [24, 25]. On the low energy side a long-exponential band tail is observed, associated to structural disorder, which introduces localized levels and extends the band into the energy band gap [26]. The corresponding tail parameter is $E_0 \approx 0.34$ eV. By Lorentzian fitting the main peak was found to be at about 3.13 eV with FWHM $\approx$ 0.19 eV and it overlaps with a small peak at about 3.28 eV with FWHM $\approx$ 0.043. No green–yellow defect band is present, which could be related to the substitutional Te in the O vacancies and passivation of the defects in the sample under treatment.

Figure 3b shows the CL image of the large structures of Fig. 3a. The image shows that CL intensity increases from the bottom to the top. CL spectra recorded at different points of the structure (Fig. 3c) show that the relative intensity of the defect band is higher in the base of the structure and decreases towards the tip. The near band edge emission appears shifted to lower energies as compared with pure ZnO which indicates the formation of the ternary compound $ZnTe_xO_{1-x}$. The peak position ranges from

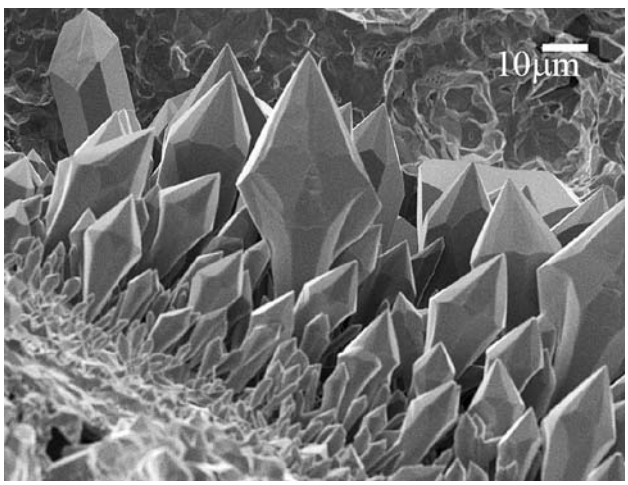

Fig. 1 Arrow-like microstructures observed in the Te-doped ZnO samples

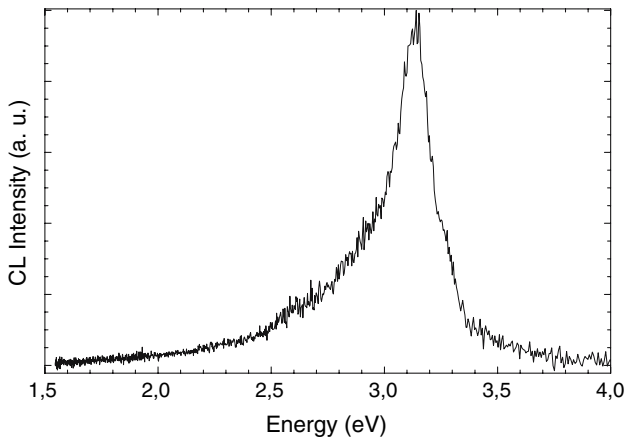

Fig. 2 Typical CL spectrum of the Te-doped ZnO sample surfaces

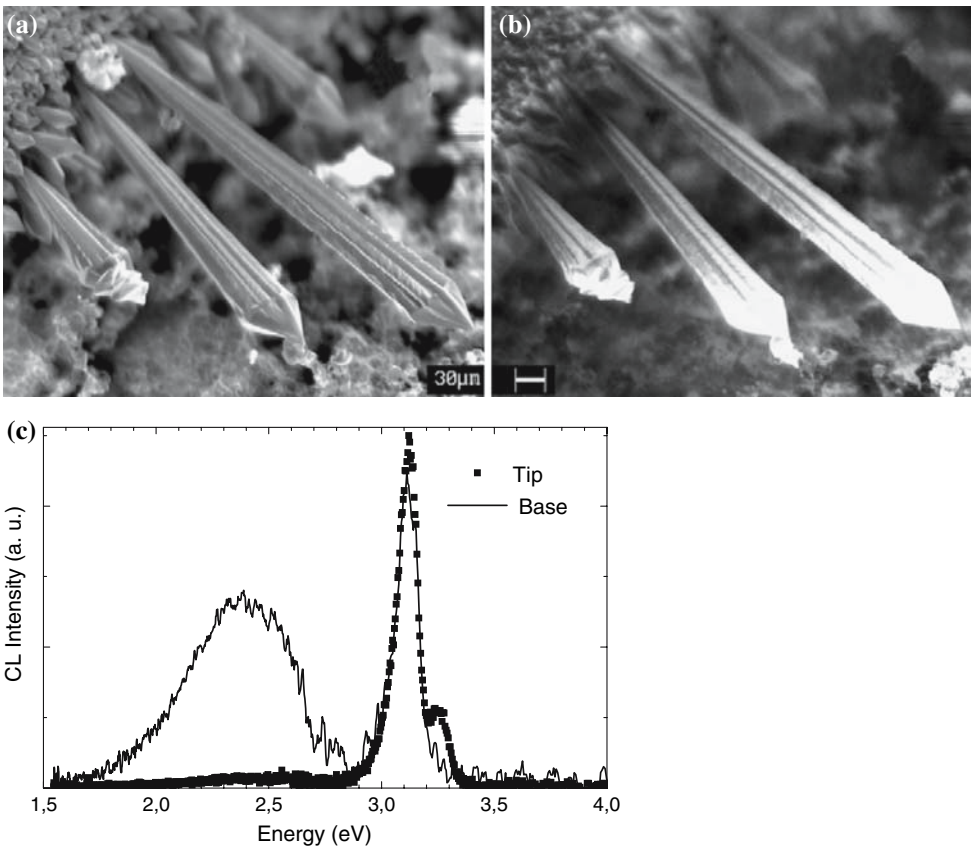

Fig. 3 SEM (**a**) and CL (**b**) images of mace-like microstructures in a Te-doped sample. (**c**) CL spectra recorded in different points of one of the structures. Te content ranges from 0% at the base to 0.09% at the tip

about 3.08 eV at the tip to 3.17 eV at the base, which according to the values of band gap for ZnO (3.26 eV) and ZnTe (2.26 eV), and using the linear approximation for the band gap energy of the ternary,

$$\mathrm{Eg}(x) = (1 - x)\mathrm{Eg}_{\mathrm{ZnO}} + x\mathrm{Eg}_{\mathrm{ZnTe}}$$

[27, 28] x values of 0.19 and 0.12 at the tip and the base, respectively, are obtained. EDS measurements performed in different positions along the axis of the structures in which the CL spectra were recorded, show the same tendency, with a lower Te signal at the base of the structures. The discrepancy of the values between CL and EDS experiments can be explained on the basis of better sensitivity of the first technique. A similar CL behaviour has been observed in the smaller arrows, as those of Fig. 1. However, the well-faceted structure of the arrow enabled EDS measurements to be performed on the different facets. The results are shown in Fig. 4, and show that the Te incorporation is a function of the face.

The fact that the relative intensity of the deep level band decreases towards the tip would indicate a reduced contribution of oxygen vacancies, involved in this emission [19, 20] which supports the incorporation of Te in O sites.

A different behaviour is observed in the hedgehog-like structures shown in Fig. 5. They are formed by needle-like (A) and pencil-like (B) structures, with aspect ratio of about 30, which show high-luminescence intensity. The CL spectra show that the defect band is practically absent and the intensity of the band edge emission decreases and its width (FWHM) increases as we move towards the tip. An analysis of the low energy side of this band gives exponential behaviour, which corresponds to the presence of a band tail. The tail parameter E_0 ranges from about 100 meV in the base to 470 meV in the tip, which means that the

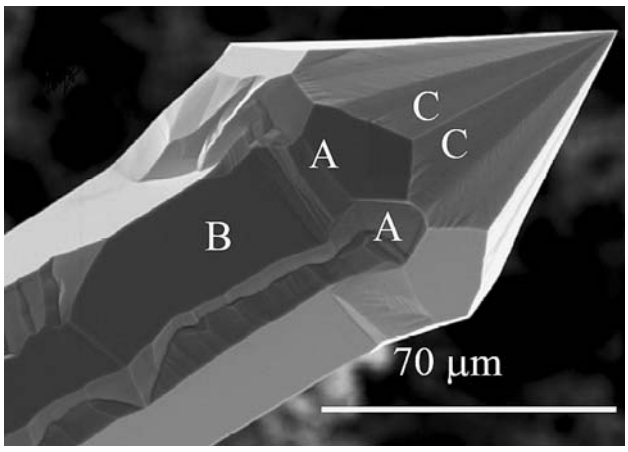

Fig. 4 SEM image of arrow-like structures. Te content estimated from EDS spectra recorded on different faces is indicated (A faces 0% Te; B faces: 0.09% Te; and C faces: 0.26% Te)

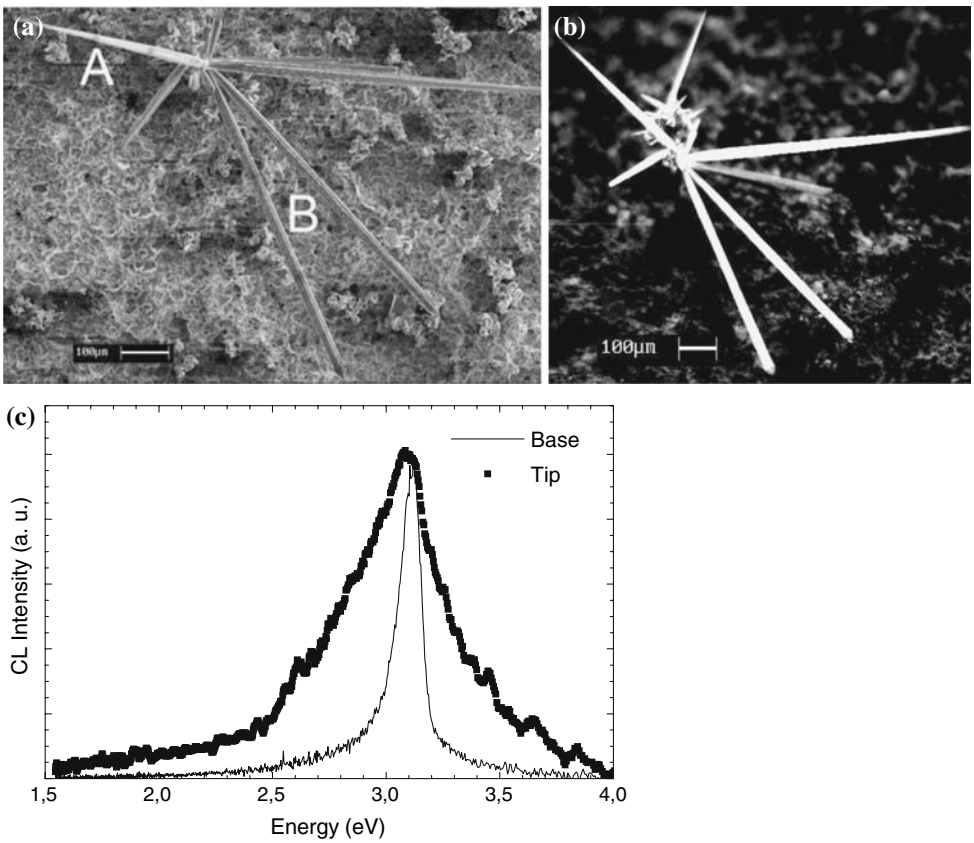

Fig. 5 (**a**) SEM image of a group of needle-like (A) and pencil-like structures (B); (**b**) CL image of the same group; and (**c**) CL spectra recorded along one of the needles

structural disorder increases from base to tip. EDS experiments do not detect the presence of Te although the shift of the band edge peak with respect to the value of ZnO suggest the formation, albeit to a little extent, of the ternary compound. The non-radiative levels associated to the structural disorder present in these structures would compete with some other kinds of defects, thus decreasing the intensity of CL.

Conclusions

Te-doped ZnO-elongated microstructures have been grown by a vapour–solid process. CL and EDS show the incorporation of Te in the microstructures. Arrow-shaped structures show an increase in Te content from the base to the tip and a corresponding enhancement of the near band edge emission and a reduction of the defect band. It is suggested that this is due to the Te incorporation in O sites. The incorporation of Te has been also found to depend on the facet of the elongated structure.

Acknowledgements One of the authors (A.I.) would like to thank MEC Spain and UCM for mobility financing and facilities under SAB2005-0018. This research was partially supported by Project MAT2006-01259.

References

1. Makino T, Tamura K, Chia CH, Segawa Y, Kawasaki M, Ohtomo A, Koinuma H (2002) J Appl Phys 92:7157
2. Tan ST, Chen BJ, Sun XW, Fan WJ, Kwok HS, Zhang XH, Chua SJ (2005) J Appl Phys 98:013505
3. Pearton SJ, Norton DP, Ip K, Heo YW, Steiner T (2005) Progr Mater Sci 50:293
4. Shim M, Wang C, Norris DJ, Guyot-Sionnest P (2001) MRS Bull 1005
5. Dalpian GM, Chelikowsky JR (2006) Phys Rev Lett 96:226802
6. Galli G (2005) Nature 436:32
7. Erwin SC, Zu L, Haftel MI, Efros AL, Kennedy TA, Norris DJ (2005) Nat Lett 436:91
8. Baltramiejunas R, Ryzhikov VD, Gavryushin V, Kazlauskas A, Raciukaitis G, Silin VI, Juodzbalis D, Stepankevicius V (1992) J Luminescence 52:71
9. Grym J, Fernández P, Piqueras J (2005) Nanotechnology 16:931
10. Maestre D, Cremades A, Piqueras J (2004) J Appl Phys 97:044316
11. Nogales E, Méndez B, Piqueras J (2005) Appl Phys Lett 86:113112
12. Hidalgo P, Méndez B, Piqueras J (2005) Nanotechnology 16:2521
13. Magdas DA, Cremades A, Piqueras J (2006) Appl Phys Lett 88:113107
14. Khomenkova L, Fernández P, Piqueras J (2007) Crystal Growth Design 7:836
15. Piqueras J, Kubalek E (1985) Sol Stat Comm 54:745
16. Vanheusden K, Warren WL, Seager CH, Tallant DR, Voigt JA, Gnade BE (1996) J Appl Phys 79:7983

17. Dingle R (1969) Phys Rev Lett 23:579
18. Tatsumi T, Fujita M, Kawamoto N, Sasajima M, Horikoshi Y (2004) Jpn J Appl Phys 43:2602
19. He H, Wang Y, Zou Y (2003) J Phys D Appl Phys 36:2972
20. Radoi R, Fernández P, Piqueras J, Wiggins MS, Solis J (2003) Nanotechnology 14:794
21. Porter HL, Muth JF, Narayan J, Foreman JV, Everitt HO (2006) J Appl Phys 100:123102
22. Ortega Y, Fernández P, Piqueras J (2007) Nanotechnology 18:115606
23. Jin BJ, Im S, Lee SY (2000) Thin Solid Films 366:107
24. Castaing O, Granger R, Benhlat JT, Lemoine D, Verdy O, Triboulet R (1995) Semicond Sci Technol 10:983
25. Bürger H, Kneipp K, Hobert H, Vogel W, Kozhukharov V (1992) J Non-Cryst Sol 151:134
26. Iribarren A, Castro-Rodríguez R, Caballero-Briones F, Peña JL (1999) Appl Phys Lett 74:2957
27. Amutha R, Subbarayan A, Sathyamoorthy R (2006) Cryst Res Technol 41(12):1174
28. Rakhshani AE (2004) Semicond Sci Technol 19:543